HHS Public Access

Author manuscript

Nat Neurosci. Author manuscript; available in PMC 2016 November 02.

Published in final edited form as:

Nat Neurosci. 2016 June ; 19(6): 788–791. doi:10.1038/nn.4301.

In-vivo imaging of dendritic pruning in dentate granule cells

J. Tiago Gonçalves, **Cooper W. Bloyd**, **Matthew Shtrahman**, **Stephen T. Johnston**, **Simon T. Schafer**, **Sarah L. Parylak**, **Thanh Tran**, **Tina Chang**, and **Fred H. Gage**

Laboratory of Genetics, Salk Institute for Biological Sciences, La Jolla, CA

Abstract

We longitudinally imaged the developing dendrites of adult-born mouse dentate granule cells (DGCs) in vivo and found that they underwent over-branching and pruning. Exposure to an enriched environment (EE) and constraining dendritic growth by disrupting Wnt signaling led to increased branch addition and accelerated growth, which were, however, counteracted by earlier and more extensive pruning. Our results indicate that pruning is regulated in a homeostatic fashion to oppose excessive branching and promote a similar dendrite structure in DGCs.

In the rodent brain the dentate gyrus (DG) of the hippocampus incorporates newborn neurons through adulthood [1]. Adult-born DGCs arise from a neurogenic niche in the subgranular zone and migrate a short distance radially into the granular layer as they differentiate and extend dendrites to form functional synapses in the molecular layer [2,3]. They recapitulate the developmental steps of perinatally born DGCs [4] and are indistinguishable from the latter after maturation [5]. Adult neurogenesis in the DG is strongly modulated by experience, with both exposure to EEs and voluntary exercise resulting in an increase in newborn cells [6,7]. However, whether adult-born DGCs undergo a period of dendrite overgrowth and subsequent pruning, and whether this process is modulated by experience, remain unknown. To address this question, we imaged DGC dendrites recurrently and longitudinally over a period of several weeks to trace the fate of individual branches. This approach allowed us to investigate the effects of experience and molecular cues on the addition and pruning of dendrite branches during development.

To image the dendritic development of adult-born DGCs, we placed a glass-bottomed implant on the hippocampal fissure (Fig. 1a). Histological analysis of chronically implanted brains (Supplementary Fig. 1a,b) confirmed that the DG boundary was preserved and that adult-born cells integrated into the DG. Importantly, perforant path inputs to the DG were not severed, and DGC activation patterns following exposure to a novel EE were not altered in hippocampi with DG implants. (Supplementary Fig. 1c,d).

Corresponding author: Fred H. Gage (gage@salk.edu).

Author Contributions:

J.T.G. and F.H.G. conceived the project, designed experiments and wrote the manuscript. J.T.G., C.W.B., S.T.J., S.T.S., S.L.P., T.T., T.C. carried out experiments. J.T.G., C.W.B., M.S. and S.L.P. analyzed the data. J.T.G., S.T.J. and F.H.G. co-developed the DG ‘window’ implant technique. F.H.G. supervised the project.

Competing financial interests: The authors declare no competing financial interests

We selectively labeled newborn DGCs with a GFP-expressing retrovirus (RV-GFP) based on the Moloney murine leukemia virus [2,3]. Previous work has shown that the vast majority of GFP+ cells are born shortly after RV-GFP injection, so we used the time of viral infection as a birthdate reference in this study [3]. Imaging of newborn DGCs started at 15 days post-infection (dpi), when GFP expression was strong enough to image their nascent dendrites. Mice were returned to their cages between imaging sessions and the same identified cells were imaged again on a specific schedule up to 60 dpi (Fig. 1b). Sparse labeling, fiducial markers on the edge of the implant, and a coordinate system made it possible to find the same neuron over multiple imaging sessions (Supplementary Fig. 2). Z-stacks of dendritic arbors (Fig. 1c) were traced to create digital three-dimensional reconstructions that were analyzed for different morphological parameters (Fig. 1d).

We followed the development of 33 neurons in six mice over time, obtaining 366 dendrite reconstructions. DGC dendrites underwent rapid growth during the third and fourth weeks post-infection but then reached a near plateau with only small growth increments (Fig. 1e, Supplementary Fig. 3a). The early time points were characterized by a continuous addition and pruning of branches (Fig. 1d). During the third week post-infection, there was a net increase in the number of endings; however, this increase was followed by a ~28% reduction in branching during the fourth week, indicating that adult-born DGCs underwent overgrowth and dendritic pruning during their development, even though they integrated into a pre-existing network (Fig. 1f,g). By the fifth week, the number of endings was nearly unchanged; therefore, we took the 31 dpi time point as representative of the final state of the branch structure. The maximum extent of branching occurred at 21 dpi (Supplementary Fig. 3b), with a mean of 14.7 ± 0.54 endings/cell (s.e.m.). Sholl analysis revealed a broadening of the Sholl intersection curve over time, as a consequence of the overall arbor growth (Supplementary Fig. 3c). Most of the addition and pruning of branches took place in the four days around this peak (Supplementary Fig. 4a). We tracked the changes in branch structure for a subset of cells whose branches could be unambiguously matched between time points around the maximum branching. Branch addition was high on the run up to the maximum (4.0 ± 0.56 branches added/day, Supplementary Fig. 4b) but dropped sharply afterwards, whereas branch pruning tended to increase after maximum branching. The mean length of branches added between two imaging sessions was 27.8 ± 1.9 μm, which was similar to the length of pruned branches (24.3 ± 1.5 μm, Supplementary Fig. 4c). The total length added and pruned per day at these time points amounted to ~13 % of the total dendrite length at the maximum of pruning (Supplementary Fig. 4d). Although most added and removed branches tended to be between 20 and 30 μm, there was considerable variability, with the occasional addition or pruning of much larger branches (Supplementary Fig. 4e).

Having established that adult-born DGCs underwent dendritic pruning during their maturation, we next investigated whether this process was modulated by experience. Adult neurogenesis is enhanced by EE and voluntary exercise [6,7], so we followed the morphological development of 30 adult-born DGC dendritic arbors (356 reconstructions, six mice) in mice injected with RV-GFP and exposed daily to an EE with running wheels from 7 to 60 dpi (Fig. 2a, Supplementary Fig. 5a,b). The dendrites of EE mice grew faster and were longer than those of mice raised in a regular cage (RC) at 17 to 23 dpi (Fig. 2b), although the length of dendrites in the two groups converged by 31 dpi (Fig. 2c). Dendrites in the EE

group also underwent a period of overgrowth and pruning, but the maximum branching occurred four days earlier than in their RC counterparts (Fig. 2d,e). EE cells extended more branches than RC cells, peaking at 17.0 ± 0.60 endings/cell (Fig. 2f), but again, this difference was no longer present by 31 dpi, as EE dendrites pruned 35% more endings than the RC group (Supplementary Fig. 5c-e). In fact, we could find no morphological distinction between mature DGCs in EE and RC animals, with both groups having no significant differences in dendrite length or branch order (Supplementary Fig. 5f,g). The total number of Sholl intersections was higher in EE arbors at 17 dpi (maximum extent of branching), reflecting their faster growth at this age, but by 31 dpi the number of intersections was similar in both groups (Supplementary Fig. 5h,i). No significant differences were found in the rate of branch addition and pruning about maximum branching or in the sizes of added and pruned branches between EE and RC neurons (Supplementary Fig. 5j-n).

We next asked whether dendrite branching depended on the extent of dendritic growth. In the hippocampus, Wnt signaling is known to be the major regulator of adult-born DGC fate and morphogenesis [8,9], with non-canonical Wnt/Planar Cell Polarity (PCP) signaling playing a strong role in the latter. CELSR3, a core component of the Wnt/PCP pathway, regulates DGC dendritic growth [9], so we investigated how its knockdown and the consequent stunting of dendritic growth affected branching. We injected mice with a retrovirus [9] encoding GFP and a shRNA against Celsr3 (GFP+shCELSR3) and imaged the dendritic development of 26 infected DGCs (295 reconstructions, five mice; Supplementary Fig. 6a). Dendrites in the GFP+shCELSR3 (knockdown) group followed a different growth pattern from their GFP counterparts: knockdown dendrites initially grew faster but their growth also subsided earlier (Fig. 2g). By 31 dpi, knockdown dendrites were shorter than those expressing only GFP (Fig. 2h). Branching was more pronounced in the knockdown group at early time points, peaking at 17 dpi, four days earlier than the GFP-only group (Fig. 3i,j). However, the maximum number or endings was similar in both groups (Fig. 3k) and remained similar by 31 dpi despite the shorter length in the knockdown group, again highlighting that branch number is a relatively constant feature of mature DGCs. No difference was found in branch order or other morphological features, suggesting that DGCs can develop an adequate branching structure despite a disruption of dendritic growth (Supplementary Fig. 6a-e). Sholl analysis at 19 and 31 dpi reflected the faster growth at the former time point and the shorter dendrites at the latter (Supplementary Fig. 6f,g). No significant differences were found in the rate of branch addition and pruning about maximum branching or in the sizes of added and pruned branches between GFP-only and GFP+shCELSR3 neurons (Supplementary Fig. 6h-l).

How do DGC dendrites mature to a similar number of branches even if they grow in mice exposed to different environments, resulting in different extents of branching during development? The answer is that not all cells undergo the same extent of pruning. On average, the fraction of endings preserved in all cells traced is 68%, but this figure depends heavily on the maximum number of endings. Cells that extend many branches prune more than cells that extend fewer branches, both in absolute and relative terms (Fig. 3a,b,c). As a consequence, the coefficient of variation (CV) of the final number of endings is 32% smaller than the CV at the maximum of branching, that is, pruning reduces not only the number of branches but also the heterogeneity in branch numbers (Fig. 3d,e). This reduction in

heterogeneity would not occur if DGCs pruned a constant absolute number or a constant fraction of branches (Supplementary Fig. 7). Our findings therefore suggest that dendritic pruning in developing DGCs occurs in a homeostatic fashion, acting to counter excessive branching and contributing to defining a similar branch structure for all DGCs. Based on our data, we hypothesize that DGCs undergo a period of net branch overgrowth that is heavily dependent on cell-extrinsic factors, such as activity and extracellular cues [10–13], followed by a period of homeostatic branch pruning that is possibly regulated by cell-intrinsic factors [14], such as cell type-specific transcriptional programs. Furthermore, branch overgrowth with subsequent pruning occurs during both the perinatal period [15] and in adulthood. Thus, this metabolically costly[16] pattern of dendritic growth is likely essential for proper dendritic development, possibly playing a role in the selection of synaptic partners [17].

Methods

Animal use

Female C57BL/6 mice (Jackson Laboratories), six to seven weeks of age at the time of surgery, were used in this study. Unless otherwise noted, mice were group housed in regular cages (RC; 37.3cm L, 23.4cm W, 14.0cm H, InnoVive, San Diego, CA) under standard conditions, with up to five mice per cage on a 12-hour light/dark cycle. Animal allocation to different experimental groups was not randomized. Animal use and procedures were approved by the Institutional Animal Care and Use Committees of the Salk Institute and the University of California San Diego. All experiments were conducted according to the US Public Health Service guidelines for animal research.

EE

Mice assigned to EE were housed in RC from the day of surgery until 7 dpi. From that day onwards, mice were housed in groups of 5-10 in an EE cage for 12 hours/day, corresponding to the dark phase of their light cycle. The large EE cage (91 cm L, 91 cm W, 30 cm H) contained a feeder, a water dispenser, a large and a small running wheel, and multiple plastic tubes and domes. The various objects in the EE cage were kept constant throughout the experiment, and placement of the objects was altered only to the extent that the mice moved them within the cages. Daily exposure to the EE continued until the completion of imaging at 60 dpi. Whenever the mice were not in the EE cage, they were returned to RCs in groups of five for the duration of the light phase of their light cycle.

Viral injection

Adult newborn granule neurons were labeled with previously described retroviral vectors that expressed GFP expression under the control of a CAG (retrovirus chicken β-actin CMV) promoter: either RV-GFP [3] or the previously validated RV-GFP+shCELSR3 [9] was used. These viral vectors are replication incompetent and only infect cells dividing at the time of surgery. Virus titer was 10^7-10^8 colony forming units/ml. Briefly, mice were anesthetized with isoflurane (2% via a nose cone, vol/vol) and placed in a stereotaxic frame. One μl of virus solution was delivered through stereotaxic surgery to the DG of the right hemisphere of the hippocampus using a microinjector (Nanoject II, Drummond Science), at coordinates previously described [3]. Viral injection and window implantation surgery were

done within two to three hours of each other and the mice were returned to their cage and allowed to recover.

Aspiration surgery and cranial window placement

Scattering and degradation of the excitation wavefront in conventional multiphoton microscopy limit the imaging depth to ~600 μm in brain tissue [18]. This limitation can be circumvented by making a small lesion in the brain and imaging the area of interest through a narrow gradient-index (GRIN) relay lens [19] or a glass-bottomed cannula—or "window"—implant [20]. We have chosen the latter approach to image the DG since it generally allows higher resolution and greater depth of imaging. A ~3 mm diameter craniotomy was performed around the viral injection site and the cortex, the underlying dura mater was removed and the cortex, corpus callosum, and CA1 below the lesion were aspirated with a blunt tip needle attached to a vacuum line. Sterile saline was used to irrigate the lesion and keep it free of blood throughout the surgery. A 3-mm diameter, 1.7-mm deep titanium window implant with a glass bottom was placed on the hippocampal fissure This area is lined with a pial membrane that formed a border between the DG and hippocampal area CA1, allowing aspiration of the overlying cortical and CA1 tissue while keeping the DG intact. The implant was held in place with dental cement and a small titanium bar (9.5 × 3.1 × 1.3 mm) was also attached to the skull to secure the animal to the microscope stage. Following completion of the surgery, carprofen (5 mg/kg, i.p.) and buprenorphine (0.1 mg/kg, s.q.) were administrated for inflammation and analgesic relief. The mice were then allowed to recover and were returned to their cages. To address concerns about the effect of the surgical implant and imaging procedures on neuronal growth, we imaged RV-GFP-labeled newborn neurons in fixed brain sections from EE and RC mice with and without "window" implants. We found that ex vivo and in vivo data were in full accord (Fig. S6), indicating that the surgical implantation procedure and recurrent imaging had no effect on length and number of branches. Furthermore, we found that the density of dendritic protrusions on the ending segments of newborn neurons was similar in mice that underwent implant surgery and in non-implanted mice (Fig. S7).

Two-photon imaging of DGC morphology

Mice were imaged under isoflurane anesthesia (1% isoflurane in O_2, vol/vol) and head-fixed to the microscope stage via a titanium bar implant while resting on a 37° C electrical heat blanket (Harvard Instrument). Imaging of DGCs in the dorsal leaf of the DG was done with a 2-photon laser scanning microscope (MOM, Sutter Instruments) using a femtosecond-pulsed laser (Chameleon Ultra II, Coherent) tuned to 910 nm and a 40x water immersion objective (0.8 NA, Olympus). Images were acquired using the ScanImage software [21], which was written in MATLAB (MathWorks). Imaging sessions started at 15 dpi and were repeated at 17, 19, 21, 22, 23, 25, 27, 29, 31, 37, 43, 48 and 60 dpi. At each time point, we acquired a three-dimensional image stack of each GFP-expressing neuron that we followed (512 × 512 pixels; 1 μm steps), taking care to include the entirety of the dendritic tree.

Analysis and quantification of dendrite morphology

Image stacks of dendritic trees were imported in TIFF format into the Neurolucida neuron tracing software (MicroBrightField Bioscience). Cell somas and dendrites were traced

manually to ensure accurate reconstruction; dendritic arbors that could not be confidently and completely reconstructed were not used in the analysis. Dendritic reconstructions were then imported into Neurolucida Explorer (MicroBrightField Bioscience) for quantitative analysis. The dendritic parameters analyzed included the number of dendritic endings (final segments between the dendrite tip and a bifurcation), the total dendritic length (of all dendrite branches), and branch order (number of bifurcations from soma to tip of dendrites). Branch order was assigned using centrifugal numbering, and the number of branches of each order was quantified. Sholl analysis was performed by calculating the number of dendrites that intersected concentric spheres that radiated from the soma in 10-μm radius increments. Analysis of branch addition and pruning was done with the 4DSPA software[22] by visually comparing branch morphology at different time points. Data were compiled in MATLAB for further analysis. We were not able to trace all cells at all planned time points for several reasons: some cells were deemed insufficiently bright to allow the unequivocal tracing of their dendritic arbors, which happened most frequently at earlier time points; at later stages some windows were mechanically damaged or less frequently rendered opaque by bleeding. In certain instances, cells would extend one or more dendritic processes outside of the acquired field of view and could not be entirely reconstructed, or the field of view became too dense with processes from neighboring cells, preventing unambiguous reconstruction. The full list of reconstructed dendrites is included as Supplementary Table 1. Investigators had access to experimental group allocation during data acquisition and analysis.

Statistical analysis

Every DGC analyzed had a single dendritic arbor, so the number of cells was equivalent to the number of dendritic trees. All data are presented as mean ± standard error of the mean or median and inter-quartile rage (IQR, 25^{th} percentile – 75^{th} percentile). Statistical comparisons were performed in Prism 6.0 (GraphPad Software) using the Mann-Whitney U Test (MWU, one independent variable, single comparison), Wilcoxon paired rank test (paired data, one independent variable), F-test, two-way ANOVA using using either the Tukey or Sidak multiple comparison test (2 independent variables: dpi and length/endings), or Kruskal-Wallis test using Dunn's multiple comparisons test (K-W, one independent variable: type of surgery/imaging). All statistical tests were two-tailed. Threshold for significance (α) was set at 0.05. While we did not formally test data distributions for normality, we generally chose statistical tests that do not assume a normal distribution of the data. Confidence intervals for the coefficient of variation were estimated in MATLAB using standard bootstrapping techniques (bootci.m). Sample size was not determined a priori but, after overbranching and pruning were found in the RC RV-GFP experimental group, the other experiments were designed to have a similar number of cells and mice. All graph error bars represent the standard error of the mean unless otherwise specified. A supplementary methods checklist is also included.

Tissue collection

Mice were anesthetized with a lethal dose of Ketamine/Xylazine (130 mg/kg, 15 mg/kg; I.P.) and perfused transcardially with 0.9% NaCl followed by 4% paraformaldehyde (PFA) in 0.1M phosphate buffer (pH 7.4). Brains were dissected and postfixed in 4% PFA overnight.

Immunohistochemistry

All implanted mouse brains were collected for histological analysis. Fixed brains were transferred to a 30% sucrose solution for 24-72 hours to equilibrate and were subsequently frozen and sectioned coronally at 40-μm thickness on a sliding microtome. Antibodies used were rabbit anti-Iba1 (Wako Cat. No. 019-19741) at 1:1000 dilution, goat anti-FOS (Santa Cruz Cat. No. sc-48869) at 1:250 dilution, Cy3-conjugated donkey anti-rabbit IgG (Jackson Labs Cat. No. 711-165-152) at 1:250 dilution and Alexa 488-conjugated donkey anti-goat IgG (Jackson Labs Cat. No. 705-545-003) at 1:250 dilution. 4’6’-Diamidino-2-phenylindole (DAPI) was used to label nuclei. Immunofluorescence images were acquired using an Olympus confocal microscope and images were processed using ImageJ.

Fixed slice preparation and imaging

Fixed brains were transferred to Tris-buffered saline solution (TBS; 50 mM Tris-Cl, 150 mM NaCl, pH 7.5) and sectioned coronally at 350-μm thickness on a vibratome (Leica Biosystems). Imaging was done with a 2-photon laser scanning microscope (MOM, Sutter Instruments) using a femtosecond-pulsed laser (Chameleon Ultra II, Coherent) tuned to 910 nm and a 25x water immersion objective (1.05 NA, Olympus).

Data availability

The data that support the findings of this study, including all dendritic tree reconstructions, are available from the corresponding author upon request.

Supplementary Material

Refer to Web version on PubMed Central for supplementary material.

Acknowledgments

We thank Lynne Moore, Eunice Mejia, Sarah Marshall and Jacob Arroyo for their technical help. We thank Ping-Chang Lee for his help with the 4D SPA software, Cian O'Donnell for his help with analysis, and M.L. Gage for editorial comments. This work was supported by grants from The James S. McDonnell Foundation (J.T.G., S.T.J., S.T.S.,F.H.G.), CIRM Grant TB1-01175 (C.W.B.), G. Harold & Leila Y. Mathers Charitable Foundation, Annette Merle-Smith, JPB Foundation, NIH Grants MH095741 and MH092758, The Leona M. and Harry B. Helmsley Charitable Trust Grant #2012-PG-MED00 (F.H.G.), Salk Innovation Grant (M.S.) and the Lewis Biophotonics Fellowship (S.T.J.)

Abbreviations

DG	dentate gyrus
DGC	dentate granule cell
dpi	days post-infection
EE	enriched environment
GFP	green fluorescent protein
i.p.	intraperitoneal

K-W	Kruskal-Wallis test
RC	regular cage
MWU	Mann-Whitney U-test
PFA	paraformaldehyde
TBS	Tris-buffered saline
Tris	Tris(hydroxymethyl)aminomethane

References

1. Altman J, Das GD. Autoradiographic and histological evidence of postnatal hippocampal neurogenesis in rats. J. Comp. Neurol. 1965; 124:319–335. [PubMed: 5861717]
2. van Praag H, et al. Functional neurogenesis in the adult hippocampus. Nature. 2002; 415:1030–1034. [PubMed: 11875571]
3. Zhao C, Teng EM, Summers RG, Ming G, Gage FH. Distinct Morphological Stages of Dentate Granule Neuron Maturation in the Adult Mouse Hippocampus. J. Neurosci. 2006; 26:3–11. [PubMed: 16399667]
4. Espósito MS, et al. Neuronal Differentiation in the Adult Hippocampus Recapitulates Embryonic Development. J. Neurosci. 2005; 25:10074–10086. [PubMed: 16267214]
5. Laplagne DA, et al. Functional Convergence of Neurons Generated in the Developing and Adult Hippocampus. PLoS Biol. 2006; 4:e409. [PubMed: 17121455]
6. Kempermann G, Kuhn HG, Gage FH. More hippocampal neurons in adult mice living in an enriched environment. Nature. 1997; 386:493–495. [PubMed: 9087407]
7. van Praag H, Kempermann G, Gage FH. Running increases cell proliferation and neurogenesis in the adult mouse dentate gyrus. Nat. Neurosci. 1999; 2:266–270. [PubMed: 10195220]
8. Lie D-C, et al. Wnt signalling regulates adult hippocampal neurogenesis. Nature. 2005; 437:1370–1375. [PubMed: 16251967]
9. Schafer ST, et al. The Wnt Adaptor Protein ATP6AP2 Regulates Multiple Stages of Adult Hippocampal Neurogenesis. J. Neurosci. 2015; 35:4983–4998. [PubMed: 25810528]
10. Piatti VC, et al. The Timing for Neuronal Maturation in the Adult Hippocampus Is Modulated by Local Network Activity. J. Neurosci. 2011; 31:7715–7728. [PubMed: 21613484]
11. Tolwani RJ, et al. BDNF overexpression increases dendrite complexity in hippocampal dentate gyrus. Neuroscience. 2002; 114:795–805. [PubMed: 12220579]
12. Valnegri P, Puram SV, Bonni A. Regulation of dendrite morphogenesis by extrinsic cues. Trends Neurosci. 2015; 38:439–447. [PubMed: 26100142]
13. Wang L, et al. Autocrine Action of BDNF on Dendrite Development of Adult-Born Hippocampal Neurons. J. Neurosci. 2015; 35:8384–8393. [PubMed: 26041908]
14. Puram SV, Bonni A. Cell-intrinsic drivers of dendrite morphogenesis. Development. 2013; 140:4657–4671. [PubMed: 24255095]
15. Zehr JL, Nichols LR, Schulz KM, Sisk CL. Adolescent development of neuron structure in dentate gyrus granule cells of male Syrian hamsters. Dev. Neurobiol. 2008; 68:1517–1526. [PubMed: 18792070]
16. Wen Q, Chklovskii DB. A Cost–Benefit Analysis of Neuronal Morphology. J. Neurophysiol. 2008; 99:2320–2328. [PubMed: 18305091]
17. Bergami M, et al. A Critical Period for Experience-Dependent Remodeling of Adult-Born Neuron Connectivity. Neuron. 2015; 85:710–717. [PubMed: 25661179]
18. Oheim M, Beaurepaire E, Chaigneau E, Mertz J, Charpak S. Two-photon microscopy in brain tissue: parameters influencing the imaging depth. J. Neurosci. Methods. 2001; 111:29–37. [PubMed: 11574117]

19. Jung JC, Schnitzer MJ. Multiphoton endoscopy. Opt. Lett. 2003; 28:902. [PubMed: 12816240]
20. Mizrahi A, Crowley JC, Shtoyerman E, Katz LC. High-Resolution In Vivo Imaging of Hippocampal Dendrites and Spines. J. Neurosci. 2004; 24:3147–3151. [PubMed: 15056694]
21. Pologruto TA, Sabatini BL, Svoboda K. ScanImage: Flexible software for operating laser scanning microscopes. Biomed. Eng. OnLine. 2003; 2:13. [PubMed: 12801419]
22. Lee P-C, He H, Lin C-Y, Ching Y-T, Cline HT. Computer Aided Alignment and Quantitative 4D Structural Plasticity Analysis of Neurons. Neuroinformatics. 2013; 11:249–257. [PubMed: 23408326]

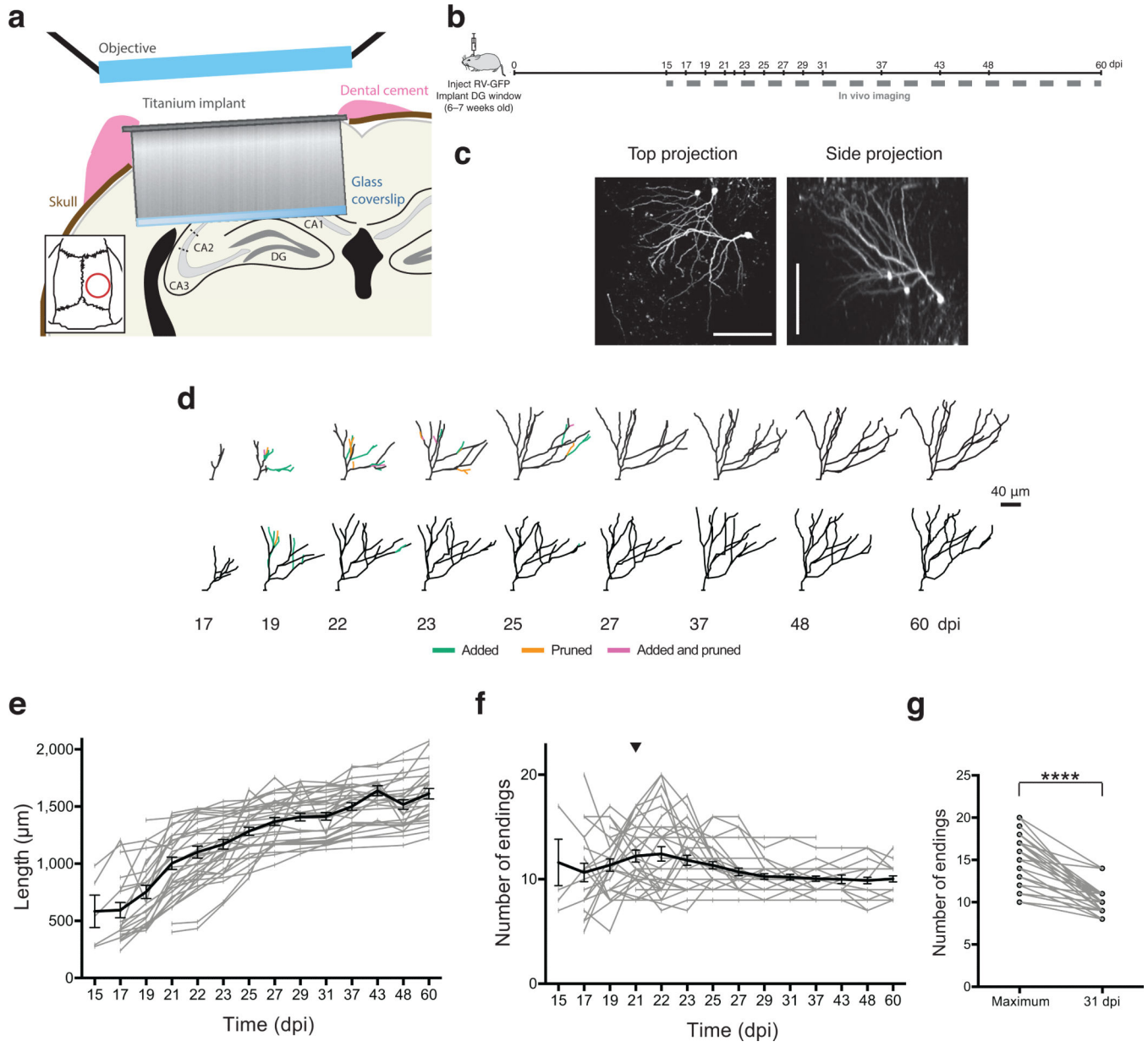

Figure 1. Chronic "window" implant enables long-term in vivo imaging of DGCs and reveals time course of overgrowth and pruning of dendritic branches

(**a**) Placement of a titanium, glass-bottomed "window" implant over the hippocampal fissure enables in vivo 2-photon imaging of the DG. (**b**) Dividing DGC progenitors were labeled with RV-GFP and the developing cells were imaged at different time points from 15 to 60 dpi. (**c**) In vivo 2-photon images of RV-GFP-labeled cells in the DG imaged 60 days post-infection. Scale bar = 100 µm. (**d**) Representative reconstructions of the dendrites of two newborn DGCs; branches added and pruned between imaging time points are highlighted. Branches in purple were absent in the previous time point and also absent in the next. Because 2-D projections are shown, some branches may be obscured at some time points. (**e**) Growth is strong during the third and fourth weeks but plateaus afterwards. (**f**) Number of endings peaks at 21 dpi (arrowhead) with 14.7 ± 0.54 dendrite endings per cell, but (**g**)

strongly decreases by 31 dpi (10.2 ± 0.27 endings per cell, $p<0.0001$, Wilcoxon paired test, n=33 cells).

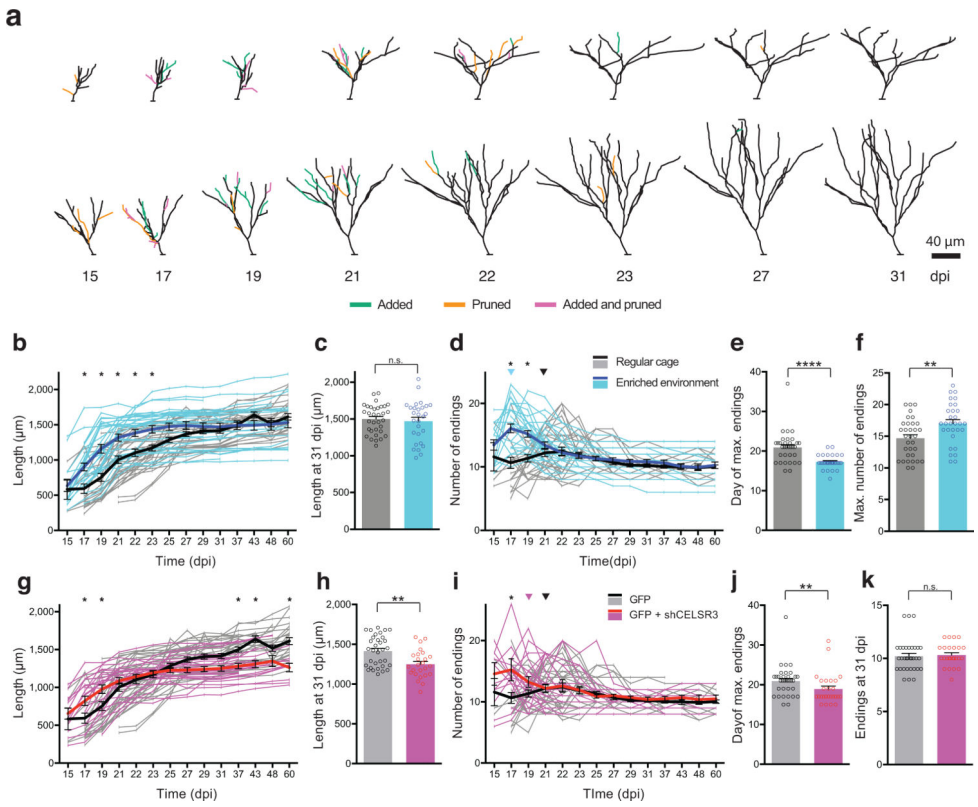

Figure 2. Exposure to EE, knockdown of CELSR3 lead to different growth and pruning time course but do not change final branch number

(**a**) Dendrite reconstruction of two DGCs from mice exposed to EE. (**b**) Individual and mean plot of dendrite length. DGC dendrites of EE mice grow faster than those of RC mice and are significantly longer from 17 dpi until 23 dpi (two-way ANOVA with Sidak correction, * $p<0.01$). (**c**) RC dendrites catch up in length to EE dendrites, and both groups have the same length by 31 dpi (WT: 1415 ± 33 µm, n=33 cells; EE: 1471 ± 52 µm, n= 28 cells; p=0.3607, MWU) (**d**) EE dendrites peak earlier (arrowhead) and have more endings than RC dendrites at 17 dpi (two-way ANOVA with Sidak correction, $P<0.001$). (**e**) Day of maximum endings (WT: 21 dpi IQR 18-22, n=33 cells; EE: 17 dpi IQR 17-19, n= 30 cells; **** $p<0.0001$, MWU). (**f**) Maximum number of endings is higher in EE dendrites (WT: 15.0 endings IQR 11.50-17.00, n=33 cells; EE: 17.0 endings IQR 17.75-19.25, n= 30 cells; ** p=0.0057, MWU). (**g**) GFP+shCELSR3 dendrites are longer at 17 and 19 dpi but their growth quickly reaches a plateau. By 37 dpi GFP-only dendrites are longer (two-way ANOVA with Sidak correction, * $p<0.05$). (**h**) Dendrite length at 31 dpi (GFP: 1415 ± 33 µm, n=33 cells; GFP +shCELSR3: 1250 ± 35 µm, n= 25 cells; * p=0.0023, MWU) (**i**) GFP+shCELSR3 dendrites reach their maximum number of endings (arrowheads) earlier than their GFP counterparts (two-way ANOVA with Sidak correction, * $p<0.01$). (**j**) Number of CELSR3-deficient endings peaks earlier than in GFP arbors (GFP: 21 dpi IQR 18-22, n=33 cells; GFP +shCELSR3: 17 dpi IQR 17-21, n= 25 cells; ** p=0.0080, MWU) (**k**) At 31 dpi, the knockdowns had the same number of endings as the GFP-only group (GFP: 10.0 endings IQR 9.0-11.0, n=33 cells; GFP+shCELSR3: 10.0 endings IQR 10.0-11.0, n= 25 cells; p=0.4238, MWU).

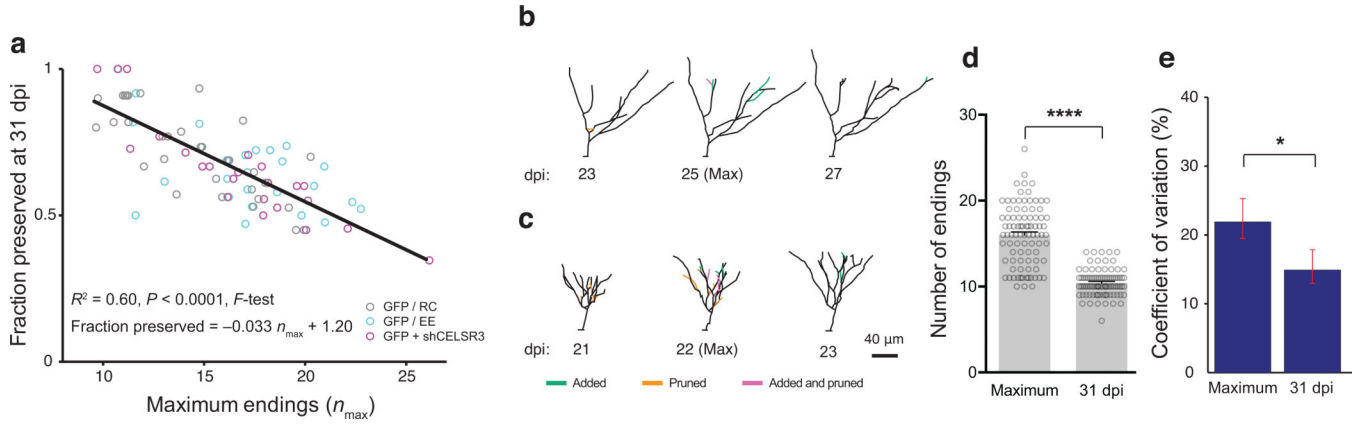

Figure 3. Pruning of DGC dendrites is homeostatic and results in reduced heterogeneity of branch numbers

(**a**) Plot of fraction of endings preserved and maximum number of endings with corresponding linear regression best-fit line (Linear regression fit: R^2 = 0.60, p<0.0001, F-test, n=86 cells, 17 mice). The fraction of endings preserved depends heavily on the maximum extent of branching. (**b**) Representative example of cell with few and (**c**) many branches around maximum branching. (**d**) Pruning results in a reduction of branches (Maximum branching: 16 endings IQR 13-18 n=89 cells; 31dpi: 10 IQR 9-11 n=86 cells, 17 mice, **** p<0.0001, MWU) but also in a significant decrease in the heterogeneity of the number of branches between cells, (**e**) as measured by the coefficient of variation (CV). Red error bars represent non-overlapping 95% confidence intervals that were calculated with standard bootstrapping methods (CV at Maximum = 21.9%, 95% C.I. = [19.5, 25.3]; CV at 31 dpi = 14.9 %, 95% C.I. = [13.0, 17.8], * p=0.0158).